Influence of the number of alkali cation on the photo-induced Co III Fe II ↔ Co II Fe III charge transfer in Cs x CoFe PBAs – A Co K-edge XANES study

Amélie Bordage, Anne Bleuzen

Influence of the number of alkali cation on the photo-induced $Co^{III}Fe^{II} \leftrightarrow Co^{II}Fe^{III}$ charge transfer in Cs_xCoFe PBAs — A Co K-edge XANES study

Amélie Bordage*, Anne Bleuzen

Institut de Chimie Moléculaire et des Matériaux d'Orsay, CNRS, Université Paris Sud, Université Paris-Saclay, 15 Rue Georges Clémenceau, 91400 Orsay, France

Abstract

In CoFe Prussian Blue Analogues (PBAs), a small difference in the number of alkali cation per unit cell can lead to drastic differences in the properties of the PBA. We investigate the origin of this effect in order to be able to control it and design new functional materials for data storage devices. Here we characterize the $Cs_{0.7}Co_4[Fe(CN)_6]_{2.8}.17H_2O$ and $Cs_2Co_4[Fe(CN)_6]_{3.3}.11H_2O$ PBAs by Co K-edge in situ XAS. For both PBAs, the photo-induced (PI) $Co^{III}Fe^{II} \rightarrow Co^{II}Fe^{III}$ charge transfer and the different involved states (room temperature, ground and PI) are described. In the case of the $Cs_{0.7}$ PBA, the relaxation from the $Co^{II}Fe^{III}$ PI state towards the $Co^{III}Fe^{II}$ ground state is monitored and quantified. All the results, fully consistent with previous magnetometry and Co L_3-edge XAS studies, are discussed with respect to the electronic structure of the Co ions in the different involved states.

Keywords: CsCoFe PBA, Alkali cation, Charge transfer, In situ XAS

1. Introduction

One of the most important challenges of today in the area of data storage devices is to transform the attractive idea of using molecular switches in the electronic industry into a realistic alternative to the currently used technology. One possibility is to use the bistability of molecular inorganic photomagnetic systems such as Prussian Blue Analogs (PBAs) of general formula $Y_xA^{II}_4[B^{III}(CN)_6]_{(8+x)/3}.nH_2O$ (A,B = transition metals; Y = alkali cation; x = 0-4). Such PBAs consist in a tridimensional network of A—NC—B linkages; the resulting face-centred cubic structure (space group $Fm\bar{3}m$) offers the possibility to incorporate alkali cations in the octants of the unit cell (between 0 and 4). This, coupled with the possibility to play with the nature of each transition metal and the alkali cation, endows PBAs with a uniquely rich range of properties.

The family of $Y_xCo_4[Fe(CN)_6]_{(8+x)/3}.nH_2O$ (called CoFe; Figure 1) PBAs is by far the most studied. Some of them indeed present a photo-induced (PI) $Co^{III}Fe^{II} \rightarrow Co^{II}Fe^{III}$ charge transfer depending on the nature and number of alkali cations inserted in the unit cell (Escax et al., 2003). For instance, CoFe PBA without alkali cation presents a $Co^{III}Fe^{II} \rightarrow Co^{II}Fe^{III}$ PI charge transfer at room temperature (RT) and 2Gpa (Cafun et al., 2012). Nevertheless, no PI charge transfer is observed at ambient pressure whatever the temperature, neither in the case of 4 alkali cations per unit cell (Bleuzen et al., 2000). On the contrary, if x=2, a PI charge transfer is observed at low temperatures whatever the nature of the alkali cation, but with some differences depending of the nature of the alkali cation (Cafun et al., 2010). In the case of Cs and Rb ions, the RT state is composed of $Co^{III}Fe^{II}$ pairs and the PI charge transfer is observed at low temperature (Bleuzen et al., 2000, 2003). In the case of Na ions, the same PI charge transfer is observed but as the RT state is composed of $Co^{II}Fe^{III}$ pairs, it is preceded on cooling from RT by a $Co^{II}Fe^{III} \rightarrow Co^{III}Fe^{II}$ thermally-induced charge transfer (Bleuzen et al., 2003; Le Bris al., 2009).

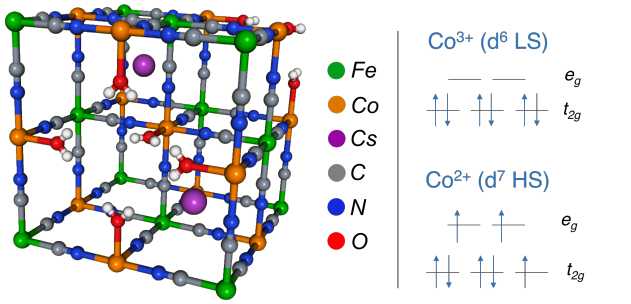

Figure 1: Scheme of a PBA unit cell (with the example of the $Cs_2Co_4[Fe(CN)_6]_{3.3}.11H_2O$, **Cs2**) and schematic representation of the electronic structure of the Co ions involved in the different states.

Among all these CoFe PBAs, the Cs derivative family was chosen to evaluate the role of the alkali cation in the photomagnetic properties of CoFe PBAs and in particular the effect of the quantity inserted in the unit cell (Bleuzen et al., 2000; Escax et al., 2001, 2003; Bleuzen et al., 2003; Ksenofontov et al., 2003; Bleuzen et al., 2004; Cafun et al., 2008, 2010). The particular cases of x=0.7 ($Cs_{0.7}Co_4[Fe(CN)_6]_{2.8}.17H_2O$, called **Cs0.7**) and x=2 ($Cs_2Co_4[Fe(CN)_6]_{3.3}.11H_2O$, called **Cs2**) were investigated in more details. The first study of **Cs0.7** focused on the characterization of its magnetic properties by SQUID magnetometry and of its RT state by Co and Fe K-edge X-ray Absorption Spectroscopy (XAS) (Escax et al., 2001) and Mössbauer spectroscopy (Ksenofontov et al., 2003); later on,

*Corresponding author
Email address: amelie.bordage@u-psud.fr (Anne Bleuzen)

its $Co^{II}Fe^{III} \rightarrow Co^{III}Fe^{II}$ thermally-induced charge transfer was investigated by Co K-edge and Cs L_3-edge XAS (Bleuzen et al., 2004). **Cs2**, which presents only a $Co^{III}Fe^{II} \rightarrow Co^{II}Fe^{III}$ PI charge transfer, was characterized by X-ray Diffraction and SQUID magnetometry (Bleuzen et al., 2003; Cafun et al., 2010); Co L_3-edge XAS was used to study both its ground and PI states (Cafun et al., 2010). We thus present here complementary data for **Cs0.7** and **Cs2** to those already published: the Co K-edge XANES spectra in the PI $Co^{II}Fe^{III}$ state for **Cs0.7** and **Cs2**, and the monitoring of the $Co^{II}Fe^{III} \rightarrow Co^{III}Fe^{II}$ charge transfer back to the ground state for **Cs0.7**. It is to be noted that in PBA, photomagnetism is due to a metal-metal charge transfer and so we recorded both the Co and Fe K-edges spectra to follow the charge transfer from each side of the cyanide bridge. Nevertheless, since (i) the energy shift of the white line between the spectra of the Co ions at the +II and +III oxidation states in PBA is much larger than that between the +II and +III oxidation states of Fe and (ii) our results are fully consistent between the Co and Fe K-edge, we present and discuss hereafter only the Co K-edge spectra.

2. Experimental method

The synthesis of both the **Cs0.7** and **Cs2** samples was described by Escax et al. (2001); the characterization of **Cs0.7** is given also by Escax et al. (2001) and the one of **Cs2** by Cafun et al. (2010). Briefly, both PBAs are obtained by reaction between an aqueous solution of potassium hexacyanoferrate(III) ($K_3[Fe^{III}(CN)_6]$) and an aqueous solution of Co(II) nitrate ($Co^{II}(NO_3)_2$); the Cs^+ ions are inserted by adding an appropriate concentration of cesium nitrate ($Cs(NO_3)$) to the ferricyanide or Co nitrate solution.

Fe and Co K-edge XAS spectra were recorded on the SAMBA beamline (Briois et al., 2011) at SOLEIL (France). We used a Si(220) monochromator in transmission mode. Samples were available as pellets. Spectra were recorded in a quick-XAS mode with both edges in a row (from 7000 up to 8700 eV) to minimize experimental artifacts. Measurements were performed at RT, at 105K and at 13K after irradiation; additional spectra were acquired at 160K in the case of **Cs0.7**. At RT and during cooling, we avoided radiation damage by using a defocused beam; low-temperature was achieved using a He-cooled cryostat and irradiation was performed with a fully focused X-ray beam. The charge transfer was monitored by measuring Co K-edge quick XANES spectra and irradiation was stopped when no more change was observed on the spectrum. The samples recovered the initial electronic structure when heated back. Following the measurements, the spectra were energy-calibrated and conventionally normalized using the ATHENA software (Ravel and Newville, 2005). Linear combination of two references was performed to evaluate the Co^{II}:Co^{III} ratio; the relative intensity of the white line peaks is compared between the linear combination spectrum and the experimental one. The $Co_4[Fe(CN)_6]_{2.7}$ PBA was used as a reference for the Co^{II} state, while the $Rb_2Co_4[Fe(CN)_6]_{3.3}$ PBA was used as a reference for the Co^{III} state (considering it consists of 80% of Co^{III} and 20% of Co^{II} (Bleuzen et al., 2000)). The estimated error on the Co^{II} and Co^{III} fractions is ±2%.

3. Results and discussion

3.1. The photo-induced charge transfer in *Cs2*

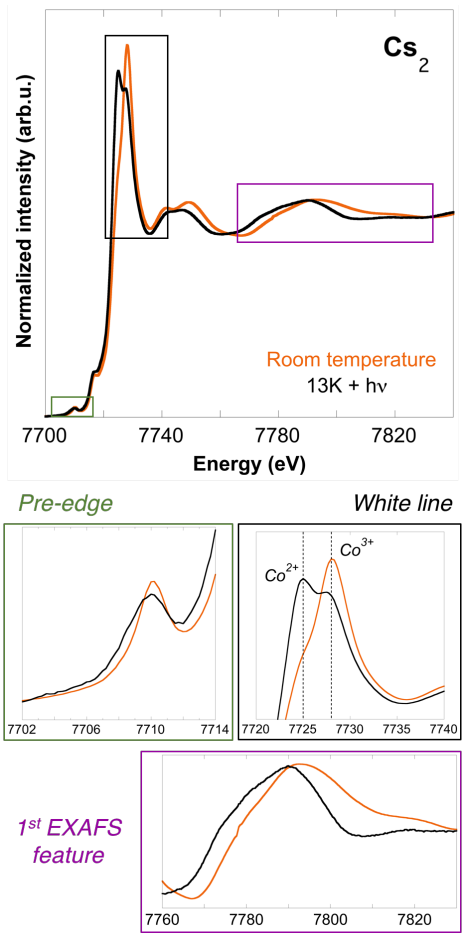

Figure 2: Normalized Co K-edge spectra of **Cs2** in its ground state (RT, orange line) and in its PI state (13K+hν, black line). The 3 insets present a zoom on the pre-edge (green), white line (black) and first EXAFS feature (purple) regions.

The normalized Co K-edge spectra of **Cs2** in its ground and PI state are displayed in figure 2, along with zooms on the pre-edge, white line and first EXAFS feature in insets.

At RT, the white line of **Cs2** is characterized by a shoulder at 7725 eV and a maximum at 7728 eV, indicating the presence of both Co^{II} and Co^{III} ions. The presence of Co^{III} ions in the ground state, even though the precursor consists in Co^{II} ions, is due to a chemically-induced electron transfer during the synthesis; this is a well known effect that occurs for a sufficient number of alkali cation inserted in the PBA (Bleuzen et al., 2000; Escax et al., 2001). In the case of **Cs2**, this chemically-induced electron transfer is total and can be detailed as $Co^{II}_4Fe^{III}_{3.3} \rightarrow Co^{II}_{0.7}Co^{III}_{3.3}Fe^{II}_{3.3}$, which corresponds to 18% of Co^{II} ions (Bleuzen et al., 2003). Upon cooling, **Cs2** remains in this $Co^{III}Fe^{II}$state, which thus corresponds the ground state of the switchable CoFe pairs.

Under irradiation at 13K, one can observe a clear increase (resp. decrease) of the Co^{II} (resp. Co^{III}) feature; this is the electronic signature of the $Co^{III}Fe^{II} \rightarrow Co^{II}Fe^{III}$ PI charge transfer that is known to occur in **Cs2** (Cafun et al., 2010). Linear combinations lead now to 65% Co^{II}, which indicates that the PI charge transfer is not complete. The variations in the pre-edge of **Cs2** are fully consistent with these changes observed on the white line and, in a simple monoelectronic view of the absorption process and the octahedral geometry of the Co ions in PBAs, they can be easily related to the electronic structure of the Co^{II} and Co^{III} ions (Figure 1). In **Cs2**, the Co^{III} ions of the ground state have a low spin (LS) configuration and the photoelectron can be promoted only to the empty e_g orbitals, resulting in one peak in the pre-edge. On the contrary, the Co^{II} ions of the PI state have a high spin (HS) configuration and the photoelectron can be promoted to both partially filled t_{2g} and e_g orbitals, resulting in two peaks in the pre-edge. The resolution of the SAMBA beamline does not allow to distinguish two well separated peaks in the pre-edge of the PI state, but we can clearly observe a single peak in the ground state and a broader peak towards lower energy in the PI state which can be described as the envelop of the expected two peaks. The shift of the first EXAFS feature towards lower energy when the quantity of Co^{II} ions increases is also fully consistent with the electronic structure of the Co^{II} and Co^{III} ions and the related structural variations arising from the PI charge transfer. In the case of the Co^{II}(HS) ions, the anti-bonding e_g orbitals are partially occupied, leading to an increase of the Co-to-ligand distance. According to Natoli's rule (Bianconi et al., 1983), this increase of the distance is reflected on the spectrum by a shift towards lower energy of the EXAFS first feature, as observed on our experimental spectra.

*3.2. The photo-induced charge transfer in **Cs0.7***

The normalized Co K-edge spectra of **Cs0.7** are displayed in figure 3, along with zooms on the pre-edge, white line and first EXAFS feature in insets.

At RT, **Cs0.7** is composed of $Co^{II}Fe^{III}$ pairs, as shown by the single peak observed in the white line at 7725 eV. The quantity of inserted Cs ions is indeed too small to lead to the chemically induced charge transfer observed for **Cs2**. This $Co^{II}Fe^{III}$ state is defined as its RT state.

At 105K, noticeable changes are visible on the spectrum: the intensity of the Co^{II} feature decreases and a shoulder at 7728 eV has appeared, indicating the presence of Co^{III} ions (comparison with references gives 23% of Co^{III}). The presence of the two oxidation states is reflected also in the changes of the pre-edge and first EXAFS features. In the pre-edge, the peak is less broad and slightly shifted towards higher energy, consistently with the electronic structure of Co^{III}(LS) ions, as explained for **Cs2**. For the EXAFS feature, it is clearly shifted towards higher energy; this is consistent with the presence of Co^{III} ions and an average Co-to-ligand distance shorter than in the RT state where only Co^{II} ions were present. This thermally-induced $Co^{II}Fe^{III} \rightarrow Co^{III}Fe^{II}$ charge transfer in **Cs0.7** is well-known and was already investigated by X-ray diffraction, SQUID magnetometry, Co K-edge and Cs L_3 edges XAS (Escax et al., 2001; Bleuzen et al., 2003, 2004); the spectral observations described here are in agreement with these previous results.

This $Co^{II}Fe^{III} \rightarrow Co^{III}Fe^{II}$ charge transfer upon cooling from RT thus enables to reach the $Co^{III}Fe^{II}$ ground of the photoswitchable CoFe pairs, which in turn allows for a $Co^{III}Fe^{II} \rightarrow Co^{II}Fe^{III}$ PI charge transfer. This was first observed by SQUID magnetometry (Escax et al., 2001) but it is the first time that this PI charge transfer in **Cs0.7** is monitored by Co K-edge XAS. The first change on the spectra between the ground state at 105K and the PI one at 13K+hν is the disappearance of the shoulder at 7728 eV: after irradiation, a single peak at 7725 eV is visible in the white line, indicating that all the $Co^{III}Fe^{II}$ pairs of the ground state switched back to $Co^{II}Fe^{III}$. The pre-edge peak is also close to the one of the $Co^{II}Fe^{III}$ RT state, with a broader peak and a lower energy with respect to the pre-edge of the ground state, in agreement with the electronic structure of the Co^{II}(HS) ions (Figure 1) and the possible $1s \rightarrow 3d$ transitions during the absorption process. Finally, the energy position of the first EXAFS feature indicates an average Co-to-ligand distance intermediate between the ground and RT states, and very interestingly slightly smaller than in the RT state. This suggests that despite a similar electronic $Co^{II}Fe^{III}$ state in the RT and PI states, the local environment of the Co ions is a little different between these two states.

At last, we could monitor the relaxation process at 160K from the PI state (with only Co^{II} ions) to the ground one (with both Co^{II} and Co^{III} ions). Spectra were recorded every ~4 minutes, and thanks to linear combinations from references, the Co^{II}:Co^{III} ratio could be determined during the relaxation process. On the spectra (not shown here), the intensity of the Co^{II} peak in the white line progressively decreases while the one of the Co^{III} peak increases; the corresponding evolution of the % of Co^{II} and Co^{III} is displayed in figure 3. At the end of the relaxation, the relative proportion of each oxidation state was stabilized, resulting in 56% Co^{II} and 44% Co^{III}, in agreement with the 60% Co^{II} and 40% Co^{III} values determined by SQUID magnetometry for this ground state (Bleuzen et al., 2003). This confirms the reversibility of the $Co^{III}Fe^{II} \rightarrow Co^{II}Fe^{III}$ PI charge transfer, since the ground state is recovered.

4. Conclusion

For the first time, Co K-edge XAS was used to investigate the $Co^{II}Fe^{III}$ PI state of the two **Cs0.7** and **Cs2** PBAs, as well as the relaxation from the $Co^{II}Fe^{III}$ PI state towards the $Co^{III}Fe^{II}$ ground one in the case of **Cs0.7**, showing a reversibility of the process. The Co^{II}:Co^{III} ratio determined here by linear combination for the different involved states is in agreement with SQUID magnetometry analyses. The spectral characteristics of the pre-edge, white line and first EXAFS feature could all be qualitatively interpreted with respect to the electronic structure of the Co^{II}(HS) or Co^{III}(LS) ions in PBAs. A full analysis of the XANES and EXAFS spectra (i) at the Fe and Co K-edges and (ii) at the Cs L_1-edge (also recorded on SAMBA) is in progress; it will enable to compare the local environment of the transition metals involved in the charge transfer and of the alkali cation, and consequently bring crucial information on the

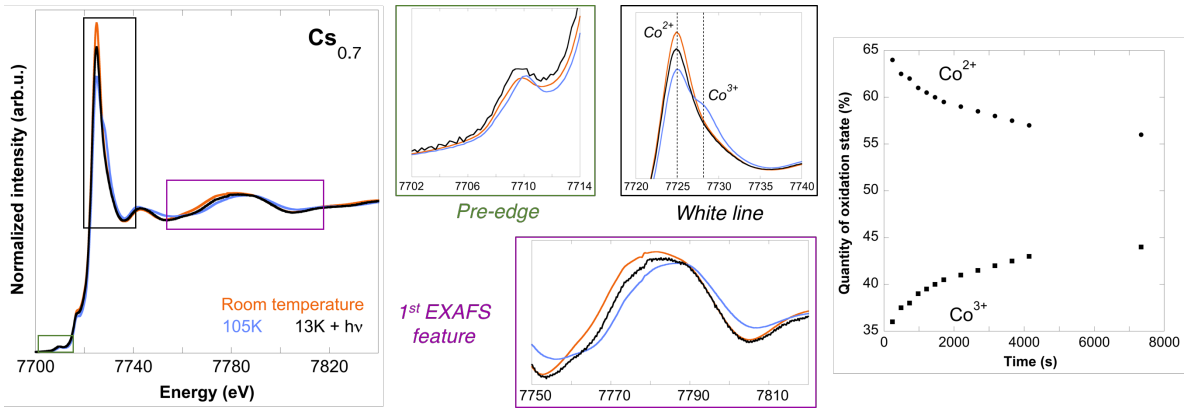

Figure 3: Normalized Co K-edge spectra of **Cs0.7** in its RT state (orange line), in its ground state (105K, blue line) and in its PI state (13K+hν, black line). The 3 insets present a zoom on the pre-edge (green), white line (black) and first EXAFS feature (purple) regions. The last inset presents the kinetics at 160K of the relaxation from the PI state towards the ground one.

role of alkali cation in the photomagnetic properties of CoFe PBA. Also, this more complete analysis will enable to understand the structural differences between the RT and PI state of **Cs0.7**, despite the electronic structure of the ions is Co^{II} (HS) in both cases. Finally, the comparison of the PI state of **Cs2** with the close $Rb_2Co_4[Fe(CN)_6]_{3.3}.13H_2O$ PBA will help to understand why the PI charge transfer is incomplete in the case of **Cs2**, even though both PBAs are in the same $Co^{III}Fe^{II}$ state.

All this information gathered on PBAs will also be of prime importance to synthesize nano- and molecular PBA-derived compound. This miniaturization of functional materials is indeed of prime importance for their use in real applications, but this requires a deep knowledge of the effect of size reduction on thermally- and PI charge transfers. A first study was thus already done on the photomagnetic $Rb_2Co_4[Fe(CN)_6]_{3.3}$ PBA synthesized as 5 nm particles embedded in the porosity of silica monolith (Moulin al., 2017; Bordage et al., 2018) and the study must now be extended to PBA with other alkali cation, such as **Cs2** investigated here. Molecular-derived Cs-PBA can also now be synthesized (Jiménez et al., 2017) and their properties must be confronted to the ones of the parent PBA.

Acknowledgments

The authors thank F. Dorchies (ICMMO), who worked on the data treatment during its internship, E. Fonda and G. Alizon (SOLEIL) for help during the experiment, and SOLEIL for the provision of the synchrotron radiation facility on the SAMBA beamline through proposal 20161363.

Bianconi, A., Dell'Ariccia, M., Gargano, A., Natoli, C.R., 1983. Bond length determination using XANES. *EXAFS and Near Edge Structure*, Springer Series in Chemical Physics (Eds Bianconi A., Incoccia A., Stipcich S., Springer, Berlin) 27, 57–61.

Bleuzen, A., Lomenech, C., Escax, V., Villain, F., Varret, F., Cartier dit Moulin, C., Verdaguer, M., 2000. Photoinduced ferrimagnetic systems in Prussian Blue analogues $C^I_xCo_4[Fe(CN)_6]_y$ (C^I = alkali cation). 1. Conditions to observe the phenomenon. J. Am. Chem. Soc. 122, 6648-6652.

Bleuzen, A., Escax, V., Itié, J-P., Münsch, P., Verdaguer, M., 2003. Photomagnetism in $C_xCo_4[Fe(CN)_6]_{(8+x)/3}.n\ H_2O$ Prussian blue analogues: looking for the maximum photo-efficiency. C. R. Chimie 6, 343-352.

Bleuzen, A., Escax, V., Ferrier, A., Villain, F., Verdaguer, M., Münsch, P., Itié, J-P., 2004. Thermally-induced electron transfer in a CsCoFe Prussian blue derivative: The specific role of the alkali-metal ion. Angew. Chem. Int. Ed. 43, 3728-3731.

Bordage, A., Moulin, R., Fonda, E., Fornasieri, G., Rivière, E., Bleuzen, A., 2018. Evidence of the core-shell structure of (photo)magnetic CoFe Prussian Blue analogue nanoparticles and peculiar behavior of the surface species. J. Am. Chem. Soc. 140, 10332-10343.

Briois, V., Fonda, E., Belin, S., Barthe, L., La Fontaine, C., Langlois, F., Ribbens, M., Villain, F., 2010. SAMBA: The 4-40 keV X-ray absorption spectroscopy beamline at SOLEIL. UVX 2010, 41-47.

Cafun, J-D., Londinière, L., Rivière, E., Bleuzen, A., 2008. Metal dilution effects on the switching properties of CoFe Prussian blue analogues. Inorg. Chem. Acta 361, 3555-3563.

Cafun, J-D., Champion, G., Arrio, M-A., Cartier dit Moulin, C., Bleuzen., A., 2010. Photomagnetic CoFe Prussian Blue Analogues: Role of the cyanide ions as active electron transfer bridges modulated by cyanide-alkali metal ion interactions. J. Am. Chem. Soc. 132, 11552-11559.

Cafun, J-D., Lejeune, J., Baudelet, F., Dumas, P., Itié, J-P., Bleuzen., A., 2012. Room-temperature photoinduced electron transfer in a Prussian Blue analogue under hydrostatic pressure. Angew. Chem. Int. Ed. 51, 9146-9148.

Escax, V., Bleuzen, A., Cartier dit Moulin, C., Villain, F., Goujon, A., Varret, F., Verdaguer, M., 2001. Photoinduced ferrimagnetic systems in Prussian Blue analogues $C^I_xCo_4[Fe(CN)_6]_y$ (C^I = alkali cation). 3. Control of the photo- and thermally induced electron transfer by the $[Fe(CN)_6]$ vacancies in cesium derivatives. 2001. J. Am. Chem. Soc. 123, 12536-12543.

Escax, V., Cartier dit Moulin, C., Villain, F., Champion, G., Itié, J-P., Münsch, P. Verdaguer, M., Bleuzen, A., 2003. Photo-induced electron transfer in ferrimagnetic Prussian blue analogues $X^I_xCo_4[Fe(CN)_6]_y$ (X^I = alkali cation). C. R. Chimie 6, 1165-1173.

Jiménez, J-R., Tricoire, M., Garnier, D., Chamoreau, L-M., von Bardeleben, J., Journaux, Y., Li, Y., Lescouëzec, R., 2017. A new $\{Fe_4Co_4\}$ soluble switchable nanomagnet encapsulating Cs^+: Enhancing the stability and redox flexibility and tuning the photomagnetic effect. Dalton Trans. 46, 15549-15557.

Ksenofontov, V., Levchenko, G., Reiman, S., Gütlich, P., Bleuzen, A., Escax, V., Verdaguer, M., 2003. Pressure-induced electron transfer in ferrimagnetic Prussian bleu analogues. Phys. Rev. B 68, 024415.

Le Bris, R., Cafun, J-D., Mathonière, C., Bleuzen, Létard, J-F., 2009. Optical and magnetic properties of the photo-induced state in the coordination network $Na_2Co_4[Fe(CN)_6]_{3.3}.14H_2O$. New J. Chem. 33, 1255-1261.

Moulin, R., Delahaye, E., Bordage, A., Fonda, E., Baltaze, J-P., Beaunier, P., Rivière, E., Fornasieri, G., Bleuzen, A., 2017. Ordered mesoporous silica monoliths as a versatile platform for the study of magnetic and photomagnetic Prussian Blue analogue nanoparticles. Eur. J. Inorg. Chem. 2017, 1303-1313.

Ravel,B., Newville, M., 2005. ATHENA, ARTEMIS, HEPHAESTUS: Data analysis for Xray absorption spectroscopy using IFEFFIT. J. Synchrotron Rad. 12, 537-541.